RESEARCH ARTICLE

Inducing 3D vortical flow patterns with 2D asymmetric actuation of artificial cilia for high-performance active micromixing

Chia-Yuan Chen · Cheng-Yi Lin · Ya-Ting Hu

Abstract Driven by the advancement of the "lab-chip" concept, a new beating behavior of artificial cilia was identified to meet the demands on rapid and complete fluid mixing in miniaturized devices. This beating behavior is characterized by an in-plane asymmetric motion along a modified figure-of-eight trajectory. A typically symmetric figure-of-eight motion was also tested for comparison. Results showed that with this new beating behavior, the mixing efficiency for complete mixing is 1.34 times faster than that with the typical figure-of-eight motion. More importantly, the required beating area was only approximately two-thirds of that in the typical figure-of-eight motion, which is beneficial for more compact designs of various "lab-chip" applications. The unique planar asymmetric motion of the artificial cilia, which enhanced the magnitudes of the induced three-dimensional (3D) flow, was identified by micro-particle image velocimetry (μPIV) measurement and numerical modeling as a major contributor in enhancing microscale mixing efficiency. Quantitatively, 3D vortical flow structures induced by the artificial cilia were presented to elucidate the underlying interaction between the artificial cilia and the surrounding flow fields. With the presented quantification methods and mixing performance results, a new insight is provided by the hydrodynamic advantage of the presented micromixing concept on efficiently mixing highly viscous flow streams at microscale, to leverage the attributes of artificial cilia in the aspect of microscale flow manipulation.

C.-Y. Chen (✉) · C.-Y. Lin · Y.-T. Hu
Department of Mechanical Engineering, National Cheng Kung University, No. 1 University Road, Tainan 701, Taiwan
e-mail: chiayuac@mail.ncku.edu.tw

1 Introduction

Miniaturized devices provide a good solution to replace traditionally time-consuming and laborious laboratory analytical assays through acceleration in processing and reduction in material consumption (Khatavkar et al. 2007) and are beneficial for biomedical/biochemical applications. A key aspect of these devices is the rapid and complete mixing of two solute streams at microscale. Micromixing generally consists of three mechanisms for mass transfer, namely molecular, eddy, and bulky diffusion; in the microscale flow regime, the process of micromixing is dominated by molecular diffusion only with low efficiency (Lu et al. 2002). As a remedy, an artificial cilium is applied to convert the volumes of fluids into increasingly thinning sheets of lamella, which will facilitate the diffusion and provide a promising method to accelerate the mixing process (Biswal and Gast 2004). Several successful flow manipulation applications based on the concept of artificial cilia have been reported (Evans et al. 2007; Khatavkar et al. 2007; den Toonder et al. 2008; Fahrni et al. 2009; Shields et al. 2010; Vilfan et al. 2010; Hussong et al. 2011; Chen et al. 2013a; Khaderi et al. 2013; den Toonder and Onck 2013a, b).

A cilium is a hair-like structure with a typical length of 10 μm and a diameter of 250 nm and covers the outer surface of microorganisms, such as paramecia (den Toonder et al. 2008). The collective beating of a series of biological cilia can generate a net flow with a velocity of up to 1 mm/s (Sleigh 1974). These unique beating modes

include non-reciprocal (Purcell 1977) and metachronic motions. Various beating behavior of ciliated structures is assumed to be practically useful as a flow manipulator for flow agitation in microfluidics. However, experiments on the reported artificial cilium-based micromixers are focused on illustrating various actuation methods, such as magnetic (Evans et al. 2007; Vilfan et al. 2010), electrostatic (den Toonder et al. 2008), and light-driven (van Oosten et al. 2009) forces. Minimal information is provided on the hydrodynamic interaction between artificial cilia and surrounding flow fields. Specifically, assessment on the influences of various beating behavior by artificial cilium actuation on mixing performance remains lacking. A successful discussion on this aspect can provide a good design protocol for the development of a new micromixer and shed light on various microscale flow manipulation techniques, such as micropropeller designs for propulsion applications (Downton and Stark 2009; Gauger et al. 2009). Numerical studies (Khatavkar et al. 2007; Lambert and Rangel 2010) with detailed hydrodynamics of artificial cilia are few. Only 2D flow data are shown, which lack the significant contribution of the third flow component (along the microchannel depth). The third induced flow component plays a significant role in facilitating micromixing. This finding is evidenced by a recent study, in which a new microreactor was designed to induce three-dimensional (3D) flow rotation for fluid reaction and mixing (Fang and Yang 2009). Therefore, accurately generating and further enhancing induced 3D flows while identifying the intricately hydrodynamic phenomena of artificial cilia require a good design of new microfluidic devices.

In this study, two beating behaviors of artificial cilia actuation characterized by planar symmetric and asymmetric figure-of-eight trajectories were actuated using a magnetic coil system design. This study pioneers the provision of a new beating protocol by an in-plane asymmetrical figure-of-eight trajectory, which is extremely beneficial for micromixing because of its capability to enhance induced 3D vortical flow patterns. A heavy loading on magnetic field control is generally required to actuate artificial cilia. To meet this requirement, a set of three orthogonal pairs of Helmholtz coils was fabricated in a previous study and regulated by a six-channel current source for the motion actuation of artificial cilia along arbitrary directions (Vilfan et al. 2010). Moreover, a set of quadruple coils was assembled to create a rotating magnetic field for flow actuation through artificial cilium actuation (Fahrni et al. 2009). An alternative method with less effort on magnetic field control for artificial cilium actuation (Evans et al. 2007) is by circulating a permanent magnet beneath the artificial cilia. In this method, artificial cilia are rotated by aligning the movement of magnet (Evans et al. 2007). However, this method cannot achieve an accurate and detailed motion control. To address these drawbacks and initiate a novel mixing strategy through the actuation of artificial cilia with a relatively low magnetic control budget, a new magnetic coil system with four-coil configuration was built. An asymmetric trajectory of artificial cilia along the in-plane direction was performed using this new setup with high accuracy and less control budget.

This paper is organized as follows. A new experimental setup demonstrating various beating behavior by artificial cilium actuation for flow visualization measurement is presented in the Experimental Section. This experimental setup is followed by a pertinent deliberation on the characterization of artificial cilia by measuring their dynamic responses under a magnetic field. Micro-particle image velocimetry (μPIV) results and 3D flow fields computed by numerical modeling are described and quantitatively discussed in the Results and Discussion Section. The underlying mechanisms of these results and their associated implications in the context of microscale flow manipulation are also included. The contribution and significance of this work are summarized in the Conclusion Section.

2 Materials and methods

2.1 Fabrication of artificial cilia-based micromixer

To fabricate an artificial cilium-based micromixer, a T-shaped microchannel mold was initially fabricated by a micromachining method, where the T-shaped pattern was carved onto an acrylic substrate by micromilling. The mixing zone (in the downstream of the T-shaped microchannel) is 200 μm in width and 400 μm in depth. To embed artificial cilia in this T-shaped microchannel, a series of deep holes (10 in this case) with 50 μm diameter and 300 μm depth each was drilled along the centerline of the T-shaped microchannel. Therefore, a total of 10 artificial cilia were integrated into the micromixer. This number can be increased to enhance the mixing performance if necessary. A mixture composed of 5 μm neodymium, iron, and boron magnetic particles (MQP-15-7, Magnequench, Singapore) and polydimethylsiloxane (PDMS) solutions (Sylgard 184, Dow Corning Corp., Midland, MI, USA) was prepared and poured into these holes. This process was followed by hot baking of the microchannel for 2 days at a temperature of 60 °C for solidification. After removing the mold, the corresponding PDMS replica was enclosed by bonding via oxygen plasma surface treatment. SEM image of the fabricated microchannel with artificial cilia embedded is shown in Fig. 1.
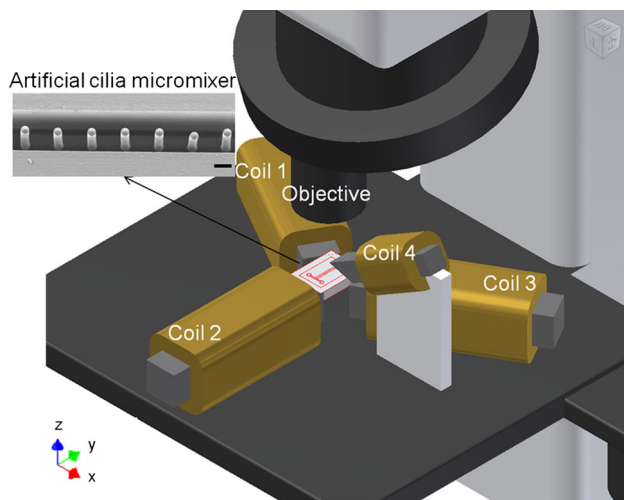
Fig. 1 Schematic illustration of the electromagnetic force in conjunction with µPIV configurations for the actuation and flow visualization of various beating behaviors of artificial cilia during micromixing. For coils *1–3*, each coil set consists of an iron rectangular bar (1.1 cm× 1.1 cm× 7.5 cm) wrapped with a single-strand 24-gauge magnetic coil at 800 turns. For coil *4*, a 0.8 cm× 0.8 cm× 4.0 cm iron bar was wrapped at 600 turns. To generate a 0.3-T magnetic field from each coil set, 20 V and 4 A were applied using an external power source. The geometrical details of the fabricated artificial cilia are shown in the SEM image on the *top left*. Each artificial cilium was 50 µm in diameter and 300 µm in height. The width and the depth of the micromixer were 200 and 400 µm, respectively. *Scale bar* is 100 µm

2.2 Magnetic coil system

To generate a homogeneous magnetic field with high controllability and to facilitate flow visualization measurement, a fourth magnetic coil with a slanted surface at its iron core tip was added to a planar three-coil configuration. This additional coil has an out-of-plane orientation (*z*-axis) with a separation angle of 45° with respect to the microscope stage. This configuration has two advantages. First, the use of solenoidal coils minimized the space required to accommodate the four sets of magnetic coils, as opposed to that required by a typical Helmholtz coil type, where a coil pair is necessary along each direction. The small space requirement can also facilitate simultaneous flow visualization measurement during artificial cilia actuation. This compact design also enhances the portable capability of the presented micromixer. Second, the actuation of arbitrary asymmetric motions of artificial cilia can be achieved by this four-coil set. This manipulation advantage constitutes the essential element for a good flow control. The layout of the magnetic actuation is illustrated in Fig. 1. A data acquisition device (NI cDAQ-9174, National Instruments, Austin, TX, USA) with modules embedded for signal inputs and outputs (NI 9201 and 9264) was connected to the coils, as well as an external power

supply (GPR-3510HD DC Power Supply, Instek, Taiwan) to facilitate the motion control of artificial cilia. An in-house script was implemented in the graphical user interface of the data acquisition device. This design concept can simplify the sophisticated magnetic control of artificial cilium actuation and be adopted by a general audience to broaden the potential applications of the design concept. For coils 1, 2, and 3, each coil set consists of an iron rectangular bar ($1.1 \times 1.1 \times 7.5$ cm) wrapped with a single-strand 24-gauge magnetic coil at 800 turns. For coil 4, a $0.8 \times 0.8 \times 4.0$ cm iron bar was wrapped at 600 turns. To generate a 0.3-T magnetic field from each coil set, 20 V and 4 A were applied using an external power source.

2.3 Beating behaviors of artificial cilia

The detailed trajectories, namely symmetric figure-of-eight (mode I) and asymmetric figure-of -eight (mode II) motions, of the two distinct beating behavior of artificial cilia tested in this study are presented in Fig. 2. The corresponding beating area was calculated as 1,632 µm² in mode I and 987 µm² in mode II on the *x–y* plane. Recording of the tip trajectories was conducted using a high-speed camera (NR4-S2, IDT, Tallahassee, FL, USA) at a speed of 100 frame/s and quantified via a kinematic software, that is, DLT dataviewer2 (Hedrick 2008). To generate mode I, in-plane coils, including coils 1, 2, and 3, were imposed by a sinusoidal wave sequentially. A phase lag between coils 1 and 3 was set as 180°, whereas that between coils 1, 2 was 270°. By superimposing the magnetic fields generated from each coil, the beating behavior of mode I was investigated. To generate mode II, coil 4 was actuated with the same frequency as other coils with the change of the phase lag relative to others. The negative values of the applied sinusoidal wave were filtered out before triggering coil 4. The rotational frequency was set as 3 Hz for all coils. Aside from the beating area calculation, to ensure that the beating behavior of the two modes was along the in-plane directions, time-dependent trajectories of a representative artificial cilium tip along the *x–z* plane were recorded and analyzed, as shown in Fig. 3. Tip displacement was plotted over time with respect to its original location for the two modes of actuation. The results showed that both modes have significant movement along the microchannel width (approximately in the range of ±30 µm), whereas almost no movement was found along the microchannel depth. Therefore, the two beating behavior only moved on the *x–y* plane (in-plane).

2.4 Micromixing task

The effectiveness of the two beating behavior was validated by accomplishing a micromixing task. This task was

Fig. 2 Actual trajectories of artificial cilia motions to demonstrate the hemodynamic advantage of artificial cilia actuation for micromixing: a figure-of-eight (*dashed line, left*) and an asymmetric figure-of-eight (*dashed line, right*). Ideal figure-of-eight trajectory is shown in *red solid line* for comparison. Beating area for actual figure-of-eight and asymmetric figure-of-eight was calculated at 1,632 and 987 μm², respectively. Units on both *x*- and *y*-axes: μm
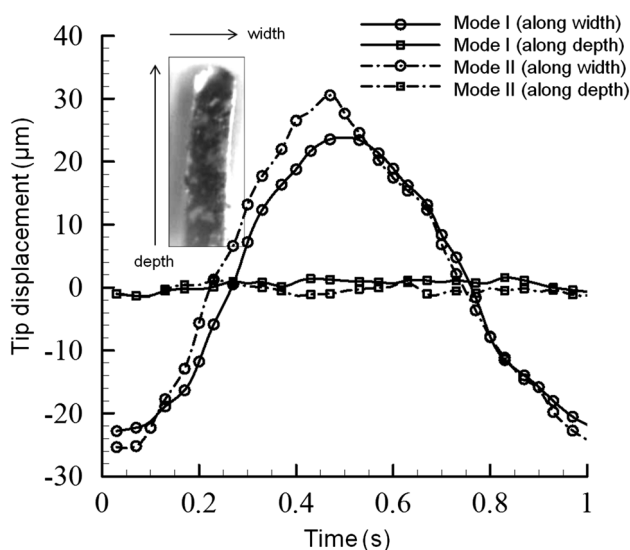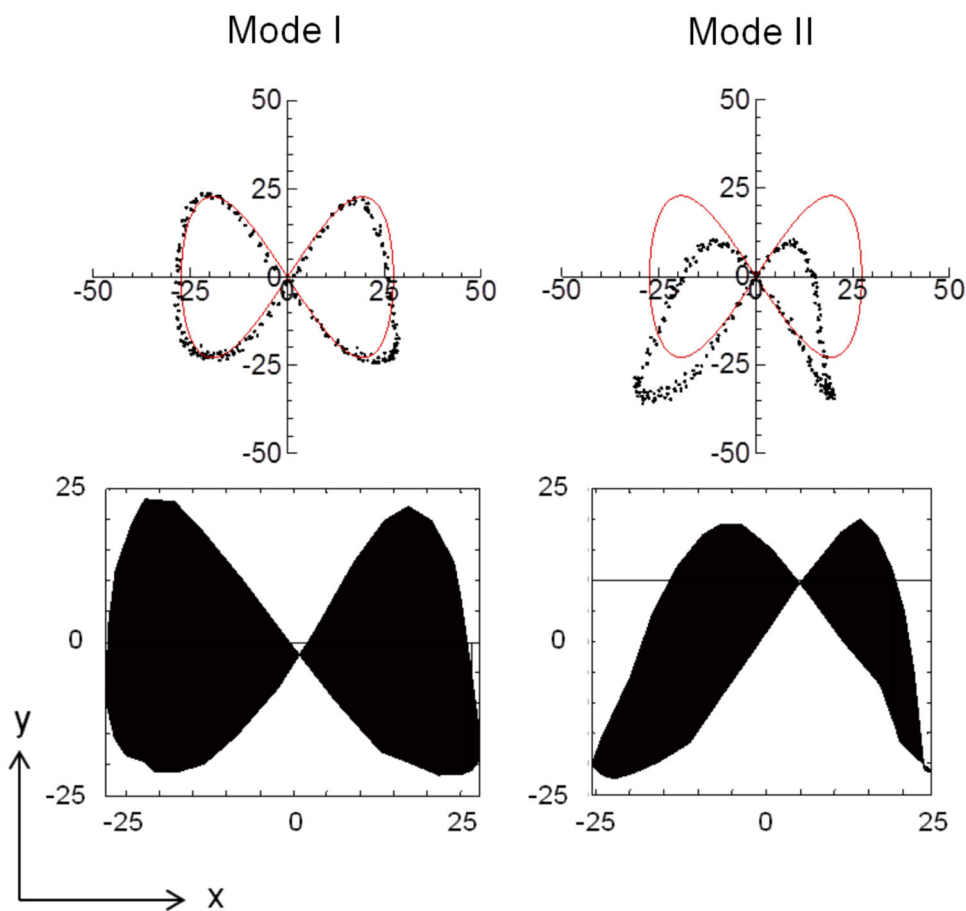

Fig. 3 Motion characterizations of artificial cilia on the transverse plane (*x–z* plane)

conducted by injecting two solutions, namely aqueous glycerol and aqueous glycerol dye solutions (red), each with 75 % weight, into the microchannel by a pressure-driven force using a calibrated syringe pump (KD Scientific, Inc.,

Holliston, MA, USA) at a total flow rate of 2.0 μL/min. The Reynolds number (*Re*) was obtained as 4.64×10^{-3}. The mixing performance of the micromixer was evaluated by measuring the intensity differences of the recorded flow mixture images in the downstream (Fang et al. 2012) at various time steps. At each time step, standard deviations of image intensity values in the downstream of the microchannel were calculated and substituted into Eq. 1 to provide quantitatively mixing performance results. Mixing performance of 1 denotes complete mixing, whereas the value of 0 refers to no mixing.

$$\text{Mixing performance} = 1 - \frac{1}{\overline{m}} \sqrt{\frac{\sum_{i=1}^{n} (m_i - \overline{m})^2}{n}} \tag{1}$$

where m_i is an intensity value of each pixel in the selected region of interest on the imaging plane, and $\overline{m}$ is the arithmetic average of m_i.

2.5 μPIV measurement and 3D numerical modeling

To provide quantitative flow patterns induced by artificial cilia, μPIV method was conducted. First, fluorescent polystyrene particles (Microgenics, Inc., Fremont, CA, USA)

with a diameter of 3.2 μm were introduced into the prepared glycerol aqueous solution under the actuation of artificial cilia. Time-dependent particle motions were imaged and recorded using a fluorescent microscope (Olympus Corp., Japan). Instantaneous flow velocity fields were subsequently calculated via a commercial PIV software, proVISION (IDT, Tallahassee, FL, USA). Velocity vectors were identified using an adaptive interrogation window method to provide a spatial resolution of 7 μm. To verify the degree of accuracy of PIV measurement conducted in this study, a validation test was performed by comparing the calculated velocity data and the theoretical solutions detailed in the Supplementary Material. This validation method was presented in our previous communication (Patrick et al. 2011; Chen and Pekkan 2013; Chen et al. 2013b). A high agreement was obtained by the comparison, which demonstrated the efficacy of PIV measurement. In the numerical modeling, a computational fluid dynamic method was employed by performing fluid–structure interaction (FSI) method and calculations using incompressible Navier–Stokes equations. The trajectories of various beating modes in addition to flow conditions were implemented in the modeling to match exact experimental boundary conditions. The induced flow structures were resolved using a commercial code, that is, ADINA (ADINA, Watertown, MA, USA). For the FSI simulation, the ciliated structure was assumed to be an isotropic linear elastic rod with a Young's modulus of 580 kPa and a Poisson ratio of 0.49. Surrounding flow was treated as a fluid with a viscosity of 0.035 Pa/s and a density of 1,184 kg/m^3. The interface between the structure and the fluid was set as an FSI interface, where the fluid force applied onto the structure and the corresponding structure deformation changed the fluid domain. The wall of microchannel was rigid with no-slip boundary conditions applied to the modeling. The movement of the ciliated structures in the modeling was primarily actuated by an imaginary force. The trajectories were designed to be identical to those measured directly from the experiment.

3 Results and discussion

3.1 Mixing performance

The micromixing performance of the two beating behavior over time is presented in Fig. 4 including the associated slope information. Real-time recordings are detailed in the Supplementary Material. In Fig. 4, no actuation of artificial cilia was performed in the first 5 s. As a result, the mixing performance was maintained at 0.4 for both modes. This phenomenon showed that an efficiently active micromixer is necessary under a viscous flow condition
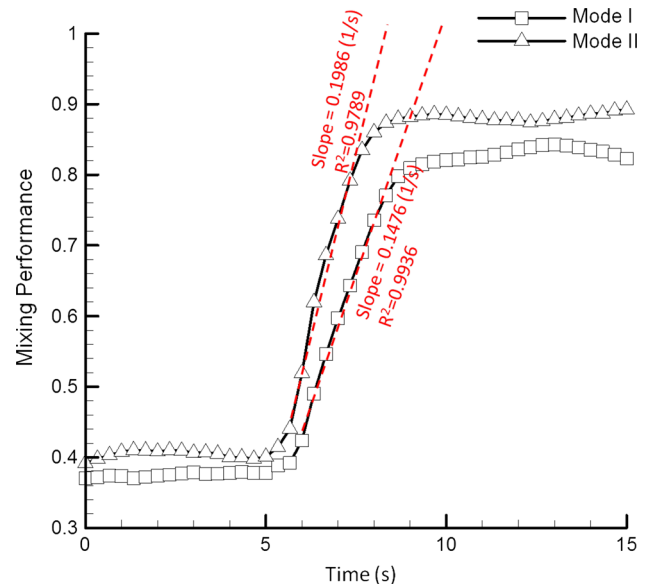

Fig. 4 Time-dependent micromixing performance of two beating behaviors

($Re = 4.64 \times 10^{-3}$) because the mixing performance is relatively low with the presence of static artificial cilia. The beating of the artificial cilia occurred in the succeeding 10 s (5–15 s) for both modes. The mixing performance increased sharply during the first half (5–10 s) of this 10-s period. During the second half (10–15 s) of the 10-s period, the mixing performance approached an asymptotic value. Differences between the mixing performances of both modes were quantified by calculating the slope values during the first half (5–10 s) of the 10-s period. The results showed that the time required for mode II to reach the highest mixing performance was 1.34 times faster than that for mode I. In addition, the highest mixing performance in mode II was evaluated as 0.88, whereas that in mode I was only 0.84.

3.2 Quantification of the induced flow fields through μPIV measurement

Compared with mode I, mode II achieved a faster mixing performance with a relatively smaller beating area required. This result opened an interesting question, that is, why a beating behavior with smaller in-plane beating area can have a better mixing performance? To provide physical insights into this finding, a flow visualization test was performed using the results shown in Fig. 5. Instantaneously induced flow velocity distribution was first measured by μPIV and subsequently calculated and presented in a form of vorticity distribution. The vorticity distribution information provides knowledge on the fluctuation of the flow based on the beating behavior of artificial cilia. In
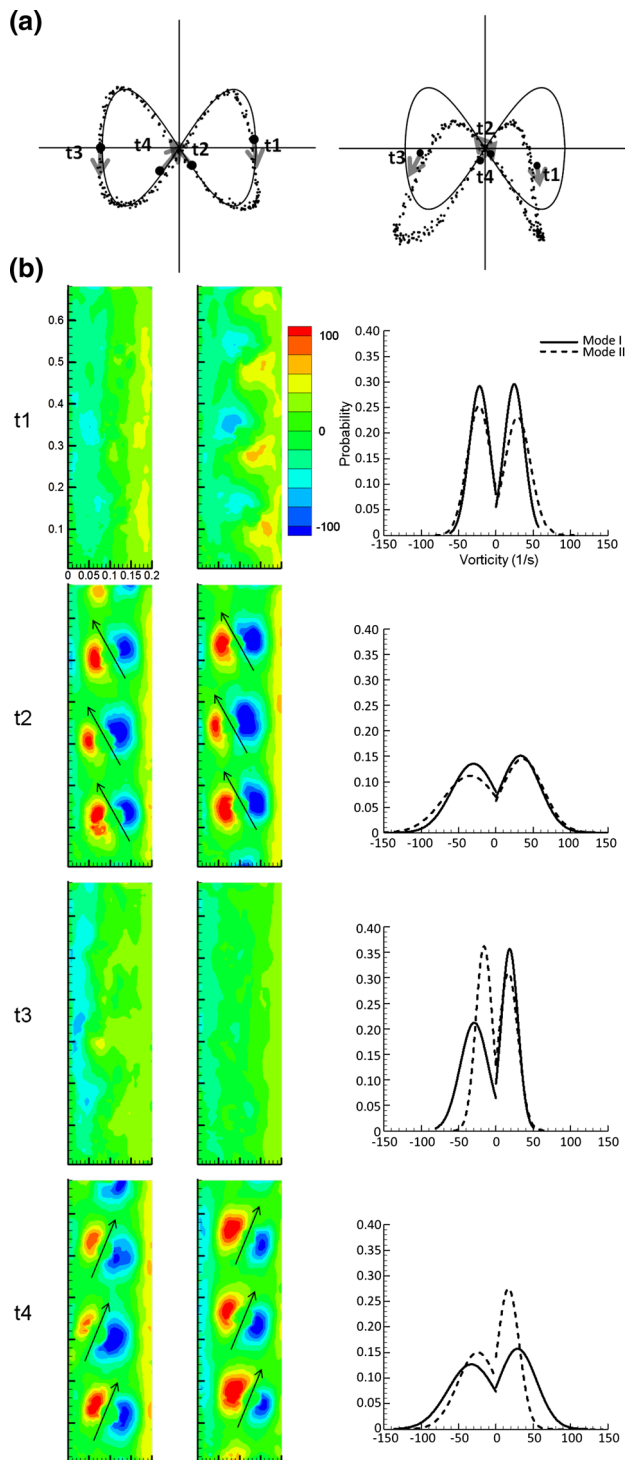
Fig. 5 Instantaneously induced in-plane flow patterns of two beating modes at four distinct time points were quantified by μPIV and presented in the form of vorticity distribution. **a** Trajectories of two modes with associated four sampling time points. **b** Calculated vorticity distribution for modes I (first column) and II (second column) and the probability density function results (third column). Unit of the *color bar*: 1/s. The induced flow direction is indicated by the *black arrow*

Fig. 5b, similar flow vorticity distribution was qualitatively observed in both modes. High vorticity magnitudes were found in both modes at time $= t_2$ and t_4, as opposed to the results presented at time $= t_1$ and t_3. This result was expected because the moving directions of the artificial cilia at time $= t_2$ and t_4 were opposite to the main flow direction. Therefore, the induced flows were also in the opposite direction with respect to the main flow direction. This opposite flow direction phenomenon led to a high vorticity generated at time $= t_2$ and t_4. By contrast, for the flow at time $= t_1$ and t_3, where the moving direction of the artificial cilia was aligned to the main flow direction, low vorticity magnitudes were obtained.

Aside from the similarity in vorticity distributions in both modes, a significant difference was observed. This difference was identified in the probability density function plot, which is also shown in Fig. 5b. A significant difference of vorticity distribution between the two modes was found at time $= t_3$ and t_4. Higher vorticity magnitudes were found in mode I than those in mode II. A hypothesis was formulated to provide a physical rationale on this flow behavior difference. The less-induced in-plane flow vorticity in mode II was assumed to be compensated by the increase of the induced flow motion along the out-of-plane direction. The rationale of this hypothesis is detailed in the following statements. At time $= t_2$, a net flow, from bottom right to top left direction (as indicated by the black arrow), was generated. This result is evidenced by the contour plot of vorticity distribution shown in Fig. 5b at time $= t_2$. Negative vorticity (colored in blue) is presented on the right-hand side, which indicates clockwise rotation of the induced flow. By contrast, positive vorticity (colored in red) is presented on the left-hand side, which indicates a counterclockwise rotation. Therefore, the induced flow was directed from the right to the left of the artificial cilia. The values for the volume of this net flow generated in both modes at time $= t_2$ were almost equal to those of the vorticity distribution of the two modes, which were approximately overlapped. Based on this analysis, an almost identical amount of flow was propelled to the left side of the artificial cilia at time $= t_2$. However, further investigation on the vorticity distribution at time $= t_3$ and t_4 showed that the vorticity magnitude and distribution were not identical in both modes. The vorticity magnitudes in mode II were smaller than those in mode I. However, the same amount of in-plane flow was induced to flow toward the left in both modes. Thus, the same amount of in-plane flow was expected to flow back to the right, in accordance with the symmetric artificial cilium motion shown in mode I and the incompressible property of the fluids. This phenomenon is supported by the probability density function

result shown in Fig. 5b in which the vorticity distribution curves (solid line) are almost identical between time $= t_2$ and t_4 in mode I. However, a different result was observed in mode II, where some of the in-plane flow was missing. The missing in-plane flow in mode II contributed to the increase of the flow fluctuation along the out-of-plane direction, which satisfied the continuity equation. However, with the current planar µPIV technique, the out-of-plane flow motion cannot be measured directly. In the subsequent paragraph, the results from the numerical modeling are presented to explain the induced flow patterns in 3D (including the out-of-plane direction).

3.3 Quantification of the induced flow fields through 3D numerical modeling

Induced flows along the out-of-plane direction were quantified numerically, as shown in Fig. 6. The out-of-plane velocity distributions along the transverse (x–z) and coronal (x–y) planes were specifically extracted and compared for both modes. Differences on the induced flow dynamics between the two modes were identified. For velocity slices along the transverse plane, as shown in Fig. 6a, out-of-plane vortical structures were observed in both modes. However, more pronounced induced flow behavior were found in mode II than those in mode I. Mode II had a negative velocity with large magnitude (colored in blue; absolute value of >0.06 mm/s), whereas mode I had a relatively low magnitude (colored in green; absolute value of <0.04 mm/s) at the same locations. Likewise, more positive velocity values with larger magnitudes were found in mode II than those in mode I. This finding supported our hypothesis that because of the asymmetric motion of artificial cilia, with the practice of mass conservation equation, the induced flow along the out-of-plane direction was more pronounced in mode II. This finding also helped elucidate the underlying mechanism of the interplay between the motion of artificial cilia and the associated induced flow behavior. Further investigation on the out-of plane velocity distribution along the coronal plane (x–y plane), as shown in Fig. 6b, c, demonstrated a unique hydrodynamic advantage that can be generated using mode II, which is also beneficial for micromixing. The out-of-plane velocity (V_z) distribution on the x–y plane was more pronounced in mode II than in mode I along the main flow direction. Phase-averaged velocity curves were also extracted from three beating cycles at time $= t_3$ (Fig. 6d) and t_4 (Fig. 6e). At time $= t_3$, mode II had more pronounced negative velocity along $\overline{dd'}$ and positive velocity along $\overline{ee'}$ than those in mode I. A similar flow trend can also be found at time $= t_4$, where mode II had more pronounced positive
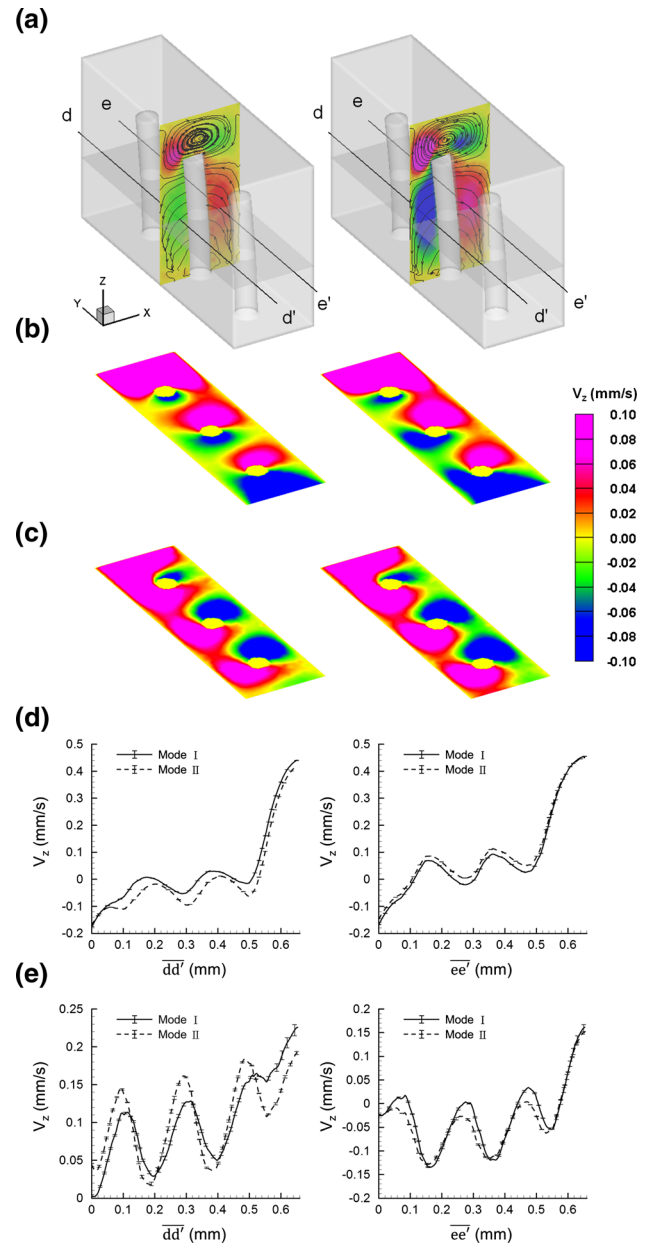

Fig. 6 Instantaneously induced out-of-plane flow patterns of two beating modes by numerical modeling. **a** Flow patterns along the sampled x–z plane at time $= t_3$ for modes I (*left*) and II (*right*). Two data extraction lines $\overline{dd'}$ and $\overline{ee'}$ are located at 50 µm away from the side wall. Flow patterns along the sampled x–y plane (150 µm above the *bottom* wall) for modes I (*left*) and II (*right*) at time $= t_3$ (**b**) and t_4 (**c**). Phase-averaged (average of three beating cycles) velocity curves along $\overline{dd'}$ and $\overline{ee'}$ for both modes at time $= t_3$ (**d**) and t_4 (**e**). *Error bars* indicate three standard deviation values of the averaged velocities from three beating cycles

velocity along $\overline{dd'}$ and negative velocity along $\overline{ee'}$. Therefore, the enhancement of the mixing performance in mode II is also attributed to a fact that a significant flow fluctuation was generated through the microchannel in mode II, which facilitated the mixing process.

To provide scientific evidence that the presented active micromixer can significantly advance the current practice of micromixing techniques, the performances of major representative micromixers in the literature were discussed and compared with the presented micromixer. The comparison between a passive micromixer and the presented active micromixer indicated that the most beneficial characteristic of the former is that it does not require any external energy to function. Therefore, this type of micromixer is widely used in contemporary "lab-chip" applications. However, most passive micromixers are limited in performance in a highly viscous flow condition. The most common operational flow condition of these micromixers is in a flow regime, where Re is in the order of 10^0–10^{-2} (Stroock et al. 2002; Nguyen and Wu 2005; Yang et al. 2009), whereas the presented micromixer can function actively when Re is only 10^{-3}. Hence, the presented micromixer is more applicable for various flow conditions than passive micromixers. Comparison of the presented micromixer to other active micromixers using different energy sources, such as pressure, electrokinetic, and acoustic energy, revealed that the presented method using magnetic force is less complicated (a handful permanent magnet can provide enough energy to facilitate the micromixing process), as opposed to other methods that require sophisticated actuation systems (Tang et al. 2002; Yaralioglu et al. 2004). Furthermore, the presented micromixer was compared with other micromixers using the same type of energy source, that is, magnetic force. The presented method can generate a flow with higher velocity than that of other methods. For instance, an artificial cilium array was fabricated by a self-assembled method (with dipole moment) and a micropatterning method in a recent study (Vilfan et al. 2010). However, the generated propelling flow is in the order of few μm/s, which is two orders of magnitude smaller than the flow speed induced in this study. This improvement is extremely important to the practical applications of commercialized microfluidic devices because the presented micromixing method increases the capability of a lab-chip to be deployed in a highly viscous flow regime. The active artificial cilium actuation method presented in this study is also particularly advantageous for flow manipulation at microscale in addition to the micromixing process. First, with the figure-of-eight planar trajectory, the out-of-plane flow can be induced solely with the in-plane motion of artificial cilia. 3D mixing and concentration of the biological/chemical solutions at microscale for microreactor applications can be achieved by applying this beating behavior. Second, by applying the in-plane asymmetric beating motion with less beating area required, flow fluctuations along the out-of-plane direction can be manifested to facilitate the mass transfer process, which is favorable for microfluidic applications necessitating a high density of compact design.

4 Conclusions

A new type of active micromixer was demonstrated through the in-plane asymmetric beating behavior of artificial cilia. A highly efficient micromixing performance was achieved using the proposed actuation concept. The induced flow patterns of the presented artificial cilium motion were characterized by μPIV and 3D numerical modeling. The hydrodynamic advantages of the beating behavior were quantified and presented, through which a 3D flow can be induced and strengthened with a small beating area required. These characteristics are beneficial for the development of next-generation micromixers. The demonstrated flow manipulation concepts may contribute to new designs of microreactors and microrobotic applications.

References

Biswal SL, Gast AP (2004) Micromixing with linked chains of paramagnetic particles. Anal Chem 76(21):6448–6455

Chen CY, Pekkan K (2013) High-speed three-dimensional characterization of fluid flows induced by micro-objects in deep microchannels. BioChip J 7(2):95–103

Chen CY, Chen CY, Lin CY, Hu YT (2013a) Magnetically actuated artificial cilia for optimum mixing performance in microfluidics. Lab Chip 13(14):2834–2839

Chen CY, Menon P, Kowalski W, Pekkan K (2013b) Time-resolved OCT-μPIV: a new microscopic PIV technique for noninvasive depth-resolved pulsatile flow profile acquisition. Exp Fluid 54:1426

den Toonder J, Onck PR (2013a) Artificial Cilia. Royal Society of Chemistry, UK

den Toonder J, Onck PR (2013b) Microfluidic manipulation with artificial/bioinspired cilia. Trends Biotechnol 31:85–91

den Toonder J, Bos F, Broer D, Filippini L, Gillies M, de Goede J, Mol T, Reijme M, Talen W, Wilderbeek H, Khatavkar V, Anderson P (2008) Artificial cilia for active micro-fluidic mixing. Lab Chip 8(4):533–541

Downton MT, Stark H (2009) Beating kinematics of magnetically actuated cilia. EPL 85(4):44002

Evans BA, Shields AR, Carroll RL, Washburn S, Falvo MR, Superfine R (2007) Magnetically actuated nanorod arrays as biomimetic cilia. Nano Lett 7(5):1428–1434

Fahrni F, Prins MW, van Ijzendoorn LJ (2009) Micro-fluidic actuation using magnetic artificial cilia. Lab Chip 9(23):3413–3421

Fang WF, Yang JT (2009) A novel microreactor with 3D rotating flow to boost fluid reaction and mixing of viscous fluids. Sens Actuat B-Chem 140(2):629–642

Fang YQ, Ye YH, Shen RQ, Zhu P, Guo R, Hu Y, Wu LZ (2012) Mixing enhancement by simple periodic geometric features in microchannels. Chem Eng J 187:306–310

Gauger EM, Downton MT, Stark H (2009) Fluid transport at low Reynolds number with magnetically actuated artificial cilia. EPJ E28(2):231–242

Hedrick TL (2008) Software techniques for two- and three-dimensional kinematic measurements of biological and biomimetic systems. Bioinspir Biomim 3(3):034001

Hussong J, Schorr N, Belardi J, Prucker O, Ruhe J, Westerweel J (2011) Experimental investigation of the flow induced by artificial cilia. Lab Chip 11(12):2017–2022

Khaderi S, Hussong J, Westerweel J, den Toonderc J, Onck P (2013) Fluid propulsion using magnetically-actuated artificial cilia—experiments and simulations. RSC Adv 3(31):12735–12742

Khatavkar VV, Anderson PD, den Toonder JMJ, Meijer HEH (2007) Active micromixer based on artificial cilia. Phys Fluids 19(8):083605

Lambert RA, Rangel RH (2010) The role of elastic flap deformation on fluid mixing in a microchannel. Phys Fluids 22(5):052003

Lu LH, Ryu KS, Liu C (2002) A magnetic microstirrer and array for microfluidic mixing. J Microelectromech Sys 11(5):462–469

Nguyen NT, Wu ZG (2005) Micromixers—a review. J Micromech Microeng 15(2):R1–R16

Patrick MJ, Chen CY, Frakes D, Dur O, Pekkan K (2011) Cellular-level near-wall unsteadiness of high-hematocrit erythrocyte flow using confocal µPIV. Exp Fluids 50:887–904

Purcell EM (1977) Life at Low Reynolds-Number. Am J Phys 45(1):3–11

Shields AR, Fiser BL, Evans BA, Falvo MR, Washburn S, Superfine R (2010) Biomimetic cilia arrays generate simultaneous pumping and mixing regimes. Proc Natl Acad Sci USA 107(36):15670–15675

Sleigh MA (1974) Cilia and flagella. Elsevier Science and Technology Books

Stroock AD, Dertinger SK, Ajdari A, Mezic I, Stone HA, Whitesides GM (2002) Chaotic mixer for microchannels. Science 295(5555):647–651

Tang ZL, Hong SB, Djukic D, Modi V, West AC, Yardley J, Osgood RM (2002) Electrokinetic flow control for composition modulation in a microchannel. J Micromech Microeng 12(6):870–877

van Oosten CL, Bastiaansen CWM, Broer DJ (2009) Printed artificial cilia from liquid-crystal network actuators modularly driven by light. Nat Mater 8(8):677–682

Vilfan M, Potocnik A, Kavcic B, Osterman N, Poberaj I, Vilfan A, Babic D (2010) Self-assembled artificial cilia. Proc Natl Acad Sci USA 107(5):1844–1847

Yang JT, Tung KY, Li CC (2009) Mixing and hydrodynamic analysis of a droplet in a planar serpentine micromixer. Microfluid Nanofluid 7(4):545–557

Yaralioglu GG, Wygant IO, Marentis TC, Khuri-Yakub BT (2004) Ultrasonic mixing in microfluidic channels using integrated transducers. Anal Chem 76(13):3694–3698